

# A Three-dimensional Error-diffusion Algorithm for Importance Sampling with Blue-noise Property

Ke Wang, Jiaojiao Zhao, Jie Feng and Bingfeng Zhou

*Institute of Computer Science and Technology, Peking University, Beijing, China*

**Keywords:** Error-diffusion, Blue-noise, Importance Sampling, Volume Rendering.

**Abstract:** We propose a novel discrete three-dimensional sampling algorithm based on the error-diffusion method, which can generate sampling points with blue-noise property. To obtain sampling points with a high quality blue-noise spectrum in 3D domain, we introduce an effective metric for the 3D blue-noise property based on 3D Fourier transform. Then, a cost function used for the search of optimal parameters, including optimal diffusion coefficients and threshold modulation strength values, is designed to guarantee the blue-noise property of sampling points. Experiments show that our algorithm is able to generate sampling points with uniform and random distribution, which possess 3D blue-noise property, and supports importance sampling in three dimensional domain. Comparing with similar work, our algorithm can achieve sampling point distribution that possesses better isotropic properties and has lower time cost in 3D discrete domain. Several applications including volume rendering and tetrahedral meshing are also explored.

## 1 INTRODUCTION

Sampling is an important technique employed in many computer graphics applications such as halftoning, rendering, vectorization, physically-based simulation and geometry processing. Early research include the Metropolis method (Metropolis et al., 1953), Poisson disk sampling (Cook, 1986) and Centroidal Voronoi Tessellation (CVT) (Du et al., 1999).

Blue-noise property refers to a sampling point distribution that is random, even and isotropic. It is characterized by a symmetrical frequency spectrum that lacks the power in low frequency. Originally blue-noise property (Ulichney, 1987) is used to measure the quality of a sampling algorithm in 2D domain. More recently, blue-noise sampling is widely used for stippling and remeshing in computer graphics (Yan et al., 2015), which extends its application to higher dimensions.

Among these high dimensional applications, volume rendering is a typical one where 3D sampling plays an important role. The volume data generated by modern 3D scanning technologies, such as CT and MRI (Novelline and Fisher, 2004), is discrete and located at regular grid points. The size of the acquired data is often drastically large, and seriously affects

the efficiency of rendering and other processing of the volume data. An optimized sampling to the volume data can greatly reduce its size, while maintaining the key features of the data. Similar works include Monte Carlo volume rendering (Csebfalvi and Szirmay-Kalos, 2003) and particle-based volume rendering (Sakamoto et al., 2007). In these studies, a point cloud of random samples is first generated and then rendered to efficiently visualize large volume data sets.

Poisson disk sampling (Dippé and Wold, 1985; Cook, 1986) is a widely used method to generate sampling points with the blue-noise property. However, the time complexity of the algorithm is high, especially when the number of sampling points is large. Recent studies, including SPH-based sampling (Jiang et al., 2015) and kernel-based sampling method (Zhong and Hua, 2016), can also be applied in 3D sampling. Error-diffusion algorithm (Floyd and Steinberg, 1976) is an important sampling method working on discrete domain. It has high efficiency, since it is independent of the number of sampling points. Zhou and Fang made some improvements on the original error-diffusion (Zhou and Fang, 2003), so that high quality sampling points with blue-noise distribution can be quickly generated.

Considering both the efficiency and the quality, we propose a three-dimensional error-diffusion algo-

---

This work is partially supported by NSFC grants #61370112, #61602012.

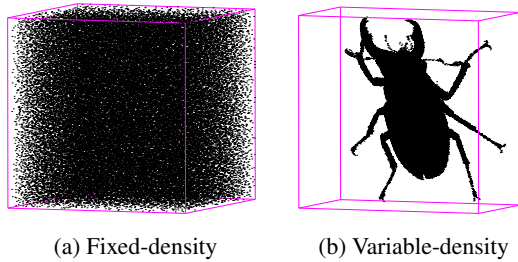


Figure 1: 3D error-diffusion sampling on discrete volume data. (a) Uniform sampling on a  $128^3$  cube with a fixed sampling density of  $g = \frac{8}{255}$ . (b) Importance sampling on a set of volume data with variable sampling density.

rithm, which extends the original 2D error-diffusion algorithm into 3D domain. Sampling points with 3D blue-noise property can be generated by optimizing the error-diffusion parameters. The algorithm is computationally efficient and experimental results show that sampling points with high quality 3D blue-noise spectrum can be obtained (Fig.1). In particular, in this paper we make the following contributions:

- We propose the framework of 3D error-diffusion, including the scanning order, the quantization threshold, the diffusion directions and diffusion coefficients.
- In order to optimize the distribution of sampling points, we introduce an effective metric of 3D blue-noise property.
- During the search of optimal parameters, a cost function is designed to obtain better blue-noise property of sampling points. Experimental results using these optimal parameters validate their effectiveness.
- We also demonstrate the applications of our method in various areas, such as volume rendering and tetrahedral meshing.

## 2 RELATED WORK

**Poisson Disk Sampling.** One of the original sampling algorithm with blue-noise property is Poisson disk sampling (Cook, 1986). A typical implementation of Poisson disk sampling is the dart throwing method (Dippé and Wold, 1985; Cook, 1986), which generates unbiased point distribution with minimum distance constraints. Tile based methods (Cohen et al., 2003; Ostromoukhov et al., 2004) improved the efficiency by sacrificing bias-free condition, which can not completely guarantee the blue-noise property of the sampling output. Other methods have been proposed to improve the performance, including hi-

erarchical dart throwing (White et al., 2007) and two phase-algorithm (Ebeida et al., 2011).

Higher dimensional sampling is also important, therefore Poisson disk sampling is extended to three, four and even higher dimensions, utilizing parallel multi-resolution uniform grid (Wei, 2008), spatial subdivision (Gamito and Maddock, 2009) and flat quadtree method (Ebeida et al., 2012). These methods are able to generate sampling points with blue-noise distribution for high dimension cases, but their performance drops rapidly as the dimension increases.

**Error-diffusion.** The original error-diffusion is an algorithm invented for generating halftone images (Floyd and Steinberg, 1976). It is also used in many other areas in computer graphics as a sampling algorithm (Alliez et al., 2002; Bourguignon et al., 2004; Kim et al., 2009). Ulichney proposed serpentine error-diffusion with threshold modulation for improving the output quality (Ulichney, 1987). According to the analysis of Knox and Eschbach (Knox and Eschbach, 1993), threshold modulation is a kind of high frequency perturbation to sampling points, which can reduce grainy effect in the sampling output. Some other research focused on ensuring the blue-noise property of sampling points, including the variable-coefficient error-diffusion (Ostromoukhov, 2001) and the variable-threshold error-diffusion algorithm (Zhou and Fang, 2003).

Unlike the error-diffusion which works directly on a discrete domain, Poisson disk sampling (Cook, 1986) is originally designed in a continuous domain and the algorithms are more complicated in higher dimensions. Hence it is not suitable for certain application areas that deal with 3D discrete domain. Error-diffusion with variable coefficients and thresholds (Zhou and Fang, 2003) can generate high quality sampling point distribution that possess blue-noise property. Moreover, the method can achieve linear time complexity by using linear scanning order. For these reasons, in this paper we propose a three-dimensional sampling algorithm based on the standard 2D error-diffusion implementations.

## 3 THREE-DIMENSIONAL ERROR-DIFFUSION

Our 3D error-diffusion is a sampling method for discrete volume data, which can generate sampling points with 3D blue-noise property. Discrete volume data, composed of a set of voxels, is a very common format for representing 3D physical signals in a dig-

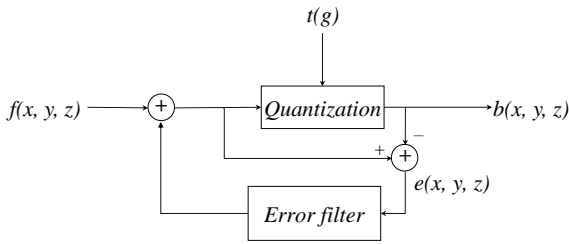


Figure 2: The framework of 3D error-diffusion. The input sampling density is quantized by a modulated threshold. The quantization error is distributed into multiple un-process voxels through an error filter, and finally results in a binary output.

ital way. The aim of our algorithm is to optimally generate sampling points that preserve characteristics of the original volume data for further processing, e.g., volume rendering and tetrahedral meshing.

For this purpose, the intensity of the volume data is first normalized and converted into a sampling density whose time complexity is linear with respect to the input data size. Hence, we assume that the input volume data is available as a finite number of density values  $g = f(x, y, z)$  located at regular grid points  $(x, y, z)$ . As described in Fig.2, the framework of 3D error-diffusion is mainly composed of two steps:

- **Quantization:** Scanning the voxels according to a specified scanning order, the quantization process compares the input density value of each voxel to a modulated quantization threshold  $t(g)$ , and return 0 if below, or 1 otherwise.
- **Diffusion:** The Quantization process produces an error  $e(x, y, z)$  that is the difference between the input and the output voxel density. Then the error is distributed into neighboring un-processed voxels through an error filter, which consists of a set of diffusion coefficients.

Then the output  $b(x, y, z)$  forms a 3D binary volume data, which includes black voxels whose density is 1, representing the sampling points, and white voxels otherwise, representing non-sampling points. Hence, there are three main issues in the 3D error-diffusion framework: (1) The scanning order; (2) The quantization threshold; (3) The error filter, i.e., the error-diffusion directions and coefficients.

**Scanning Order.** In the standard 2D error-diffusion, serpentine scanning is a commonly used scanning order (Ulichney, 1987; Ostromoukhov, 2001; Zhou and Fang, 2003), which is able to remove the directional artifact caused by uni-directional scanning. In 3D error-diffusion, the artifact should also be avoided. For this purpose, we employ a similar scheme in choosing the scanning order, which extends the serpentine scanning to three-dimensional.

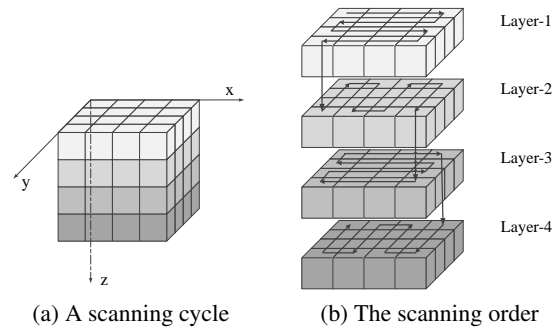


Figure 3: The rotated-serpentine scanning order. (a) A scanning cycle includes four layers of volume data. (b) Each layer adopts a different serpentine scanning direction.

Specifically, our algorithm scans voxels of the input volume in a top-bottom sequence, i.e., layers of the input voxels are processed from top to bottom one by one (Fig.3). Within each layer, voxels are scanned in a *rotated serpentine order*. To perform this, every four adjacent layers from top to bottom in the input volume are grouped as one *scanning cycle* (Fig.3(a)), where the scanning direction of 2D serpentine scanning are rotated respectively by  $90^\circ$  for each layer (Fig.3(b)).

**Quantization Threshold.** The quantization threshold is a key element in the error-diffusion algorithm. In its original form, it is a fixed value at the middle of the dynamic range of the input signal. In order to improve the blue-noise property of the output, it becomes variable by introducing a threshold modulation (Ulichney, 1987). In 3D error-diffusion, we choose a threshold modulation function that is similar with the one in the variable-threshold error-diffusion algorithm (Zhou and Fang, 2003):

$$t(g) = 0.5 + r \cdot m(g), \quad (1)$$

where  $g = f(x, y, z)$  is the density level of an input voxel,  $t(g)$  is the quantization threshold,  $m(g) \in [0, 1]$  is a density-dependent modulation strength, and  $r \in [0.0, 1.0]$  is a white-noise random number. Similar with the work (Zhou and Fang, 2003), but specific to 3D error-diffusion, here we use a different modulation strength obtained by the optimization method described in next section.

**Error-diffusion Directions and Coefficients.** In 2D domain, blue-noise property is characterized by a round shaped Fourier power spectrum. The diffusion of the errors along the diffusion directions contributes to the round shaped spectrum. Similarly, in 3D domain, blue-noise property can be characterized by a spherical shaped 3D Fourier power spectrum. In order to obtain such a spectrum, we need to choose appropriate 3D diffusion directions and coefficients

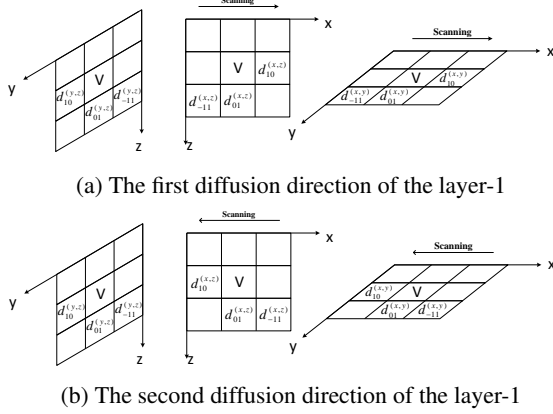


Figure 4: The diffusion directions of the layer-1 in each scan cycle.

by combining the three coordinate axes.

Specifically, for our 3D error-diffusion, there are four sets of error filter configurations, corresponding to the four rotated-serpentine scanning orders in a scanning cycle. Taking the scanning order in layer-1 as an example, we assume that current scanning direction is along the increasing direction of the  $x$  axis, and the scanning direction of  $y$  and  $z$  axis are along increasing direction of the corresponding axis, respectively. Then, the design of error filter given in the standard 2D error-diffusion (Ostromoukhov, 2001; Zhou and Fang, 2003) is applied into three coordinate planes, respectively. The corresponding configuration of diffusion directions and coefficients is shown in Fig.4. Considering the space relationship of the three filters placed on the coordinate planes, some of the coefficients are equal:  $d_{01}^{(x,y)} = d_{10}^{(y,z)}$ ,  $d_{10}^{(x,y)} = d_{10}^{(x,z)}$ , and  $d_{01}^{(x,z)} = d_{01}^{(y,z)}$ . Hence, there are totally six independent coefficients for achieving an output with blue-noise property. In our framework, these coefficients are functions of the input density, and can be determined by the optimization method given in the next section.

For other layers of the scanning cycle, the corresponding diffusion directions can be obtained accordingly by aligning the same filters on different scanning directions.

## 4 ERROR-DIFFUSION PARAMETERS OPTIMIZATION

In the case of 2D error-diffusion, metrics are developed to evaluate the quality of the blue-noise property of the output (Ostromoukhov, 2001; Zhou and Fang, 2003). In our 3D error-diffusion, similar metric is also needed to obtain optimal parameters, including dif-

fusion coefficients and threshold modulation strength values. In this section, we first define the metric of 3D blue-noise property, and then propose the method of parameter optimization based on the metric.

### 4.1 Three-dimensional Blue-noise

The property of a sampling point set can be evaluated by its Fourier power spectrum. To obtain the Fourier power spectrum, we first perform 3D Fourier transform on the sampling points, using a multi-dimensional fast Fourier transform algorithm (Press et al., 1992). Therefore, a 3D Fourier power spectrum  $\hat{P}(f)$  is calculated, where  $f$  is a 3D frequency vector.

Analogous to the definition of 2D blue-noise, 3D blue-noise also refers to the noise whose energy is absent in low frequency region, while the spectrum is symmetrical in high-frequency region. The corresponding sampling points with blue-noise property are scattered both randomly and evenly in the domain. Based on these analysis, we propose a method for measuring the blue-noise property of 3D sampling point distributions.

In (Ulichney, 1987), the *radially averaged power spectrum* and *anisotropy* are defined as the metrics of 2D blue-noise property. Similarly, we define the radially averaged power spectrum of 3D Fourier power spectrum as

$$P(f_r) = \frac{\sum_{i=1}^{N(f_r)} \hat{P}(f_i)}{N(f_r)}, \quad (2)$$

where  $N(f_r)$  is the number of frequency samples on the spherical shell of radius  $r$ . Also, the anisotropy  $anis(f_r)$  of 3D Fourier power spectrum is defined as

$$anis(f_r) = \frac{var^2(f_r)}{P^2(f_r)}, \quad (3)$$

$$var^2(f_r) = \frac{\sum_{i=1}^{N(f_r)} (\hat{P}(f_i) - P(f_r))^2}{N(f_r) - 1}. \quad (4)$$

where  $var^2(f_r)$  is the variance of the power spectrum  $\hat{P}(f)$  on the spherical shell of radius  $r$ .

To obtain a better sampling point distribution, the frequency spectrum should have a spherical symmetric distribution and lack low frequency energy, and this can be achieved by searching for optimal parameters. In the following sections, a corresponding optimization target function is described on the basis of our 3D blue-noise metrics.

### 4.2 Searching for Optimal Parameters

As the target of the optimization, the optimal parameters should lead to a symmetrical frequency spectrum,

which should be as close as possible to 3D blue-noise frequency spectrum. Derived from the 2D error-diffusion algorithm, a target function for optimal parameter searching is formulated as a weighted sum of two parts:

$$T(g) = w \cdot L(g) + (1 - w) \cdot S(g). \quad (5)$$

The first part is the *low frequency ratio*  $L(g)$ , which measures the similarity of the output spectrum with the ideal 3D blue-noise frequency spectrum. The second part  $S(g)$  is the similarity of the *segmented radially averaged power spectrums* (SRAPSS) (Zhou and Fang, 2003), which measures the symmetry of the output frequency spectrum.  $w$  is a weight ( $0 \leq w \leq 1$ ) determined according to the convergence of parameter searching.

**The Low Frequency Ratio.**  $L(g)$  is calculated as the ratio between the spectrum energy below the *principal frequency* and the energy of the whole spectrum.

For a 2D blue-noise distribution with dot density  $g$ , the relationship between the principal frequency  $f_g$  and the average dot distance  $\lambda_g$  has the form of  $f_g = 1/\lambda_g = u \cdot \sqrt{g}$ , where  $u$  is a constant (Ulichney, 1987). Similar analysis for 3D blue-noise point distributions, which can be found in Appendix A, reveals that this relationship takes a similar form in 3D domain, as given in Eq.6:

$$f_g = \begin{cases} \sqrt[3]{g} & 0 \leq g \leq 0.5, \\ \sqrt[3]{1-g} & 0.5 \leq g \leq 1. \end{cases} \quad (6)$$

Thus, the low frequency ratio  $L(g)$  for sampling points with a density level of  $g$ , can be presented by

$$L(g) = \frac{\sum_{f=0}^{f_g} \hat{P}(f)}{\sum_{f=0}^{\sqrt[3]{3/2}} \hat{P}(f)}. \quad (7)$$

Since  $L(g)$  is the ratio between the energy of low frequencies and the total energy of all frequencies, it is a value between 0 and 1. When  $L(g)$  is close to 0, it indicates that the low frequency energy of the Fourier power spectrum is close to zero. That is an important indication of 3D blue-noise property.

**The Symmetry of Frequency Spectrum.** The second part of the target function concerns the symmetry of the Fourier power spectrum. Here, we consider the symmetry of a 3D frequency spectrum in one of the eight octants, and take it as another indication of 3D blue-noise property.

We employ the concept of the segmented power spectrum from 2D error-diffusion (Zhou and Fang, 2003) and give it a new definition in 3D domain. First, the octant of the Fourier power spectrum domain is

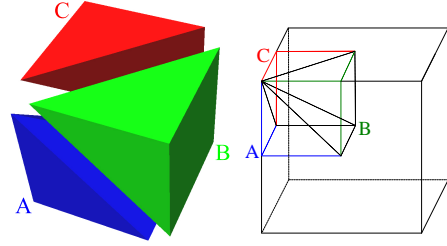


Figure 5: An octant of Fourier domain is symmetrically divided into three equal pyramids for calculating the segmented radially averaged power spectrums (SRAPSS).

divided into three equal segments which are defined by the pyramids A, B and C as shown in Fig.5. Then, for each segment, the SRAPSS are calculated as following, respectively:

$$P_{xy}(f_r) = \frac{\sum_{i=0}^{N_{xy}(f_r)} \hat{P}(f_i)}{N_{xy}(f_r)}, \quad (8)$$

$$P_{xz}(f_r) = \frac{\sum_{i=0}^{N_{xz}(f_r)} \hat{P}(f_i)}{N_{xz}(f_r)}, \quad (9)$$

$$P_{yz}(f_r) = \frac{\sum_{i=0}^{N_{yz}(f_r)} \hat{P}(f_i)}{N_{yz}(f_r)}. \quad (10)$$

Here,  $P_{xy}(f_r), P_{xz}(f_r), P_{yz}(f_r)$  are three SRAPSS corresponding to the pyramids A, B and C, and  $N_{xy}(f_r), N_{xz}(f_r), N_{yz}(f_r)$  denote the number of frequency samples for frequency  $f_r$  in the three pyramids, respectively.

We assume that correlation of these SRAPSS is an indication of the symmetry of the whole spectrum. Therefore, our similarity function  $S(g)$  of the three SRAPSS is defined as

$$S(g) = 1 - C(P_{xy}, P_{xz}, P_{yz}). \quad (11)$$

Here,  $C$  is the correlation function (Gonzalez et al., 2004) of the three curves  $P_{xy}(f_r), P_{xz}(f_r), P_{yz}(f_r)$ . The larger its value is, the more similar the curves are.

**Parameter Optimization.** With  $L(g)$  and  $S(g)$  defined, the target function  $T(g)$  in Eq.5 can be calculated. When the target function takes smaller value, the frequency spectrum is closer to a 3D blue-noise frequency spectrum. Therefore, the optimal parameters can be obtained for a given density  $g$  by minimizing  $T(g)$ .

When searching for the optimal error-diffusion parameters, we consider only the density input within  $[0, 0.5]$ . For any density  $g \in [0.5, 1]$ , the optimal diffusion parameter for the density  $1 - g$  can be directly used. It is because at this density level, we concern only the distribution of the ‘minority voxels’ of the sampling domain, whose distribution pattern is the same as that at level  $1 - g$ .

Table 1: The optimal error-diffusion parameters for key density levels.

$\hat{g}_k$	Optimal Diffusion coefficients						$m(g)$
	$A_{100}$	$A_{-110}$	$A_{010}$	$A_{0-11}$	$A_{-101}$	$A_{001}$	
1	380	79	270	62	72	59	1.00
8	525	319	719	291	132	204	1.19
16	355	202	394	171	213	110	1.09
24	338	211	240	196	164	114	1.06
32	187	179	403	132	170	144	0.99
40	163	84	394	127	236	102	1.04
48	181	90	317	75	110	154	0.93
56	114	141	446	110	211	163	1.04
64	169	99	321	101	103	154	0.89
72	225	251	221	199	54	164	0.98
80	164	209	419	236	41	179	1.06
88	130	212	498	203	54	198	1.05
96	228	209	325	140	314	380	1.01
104	173	104	368	67	65	203	0.94
112	122	184	436	109	234	166	1.09
120	75	225	535	82	129	236	1.02
127	366	322	324	80	125	283	1.23

In order to reduce the computational complexity, we only calculate optimal parameters for a group of selected *key density levels*. For each key density level, the optimal parameters are found by minimizing  $T(g)$  with a simplex optimization algorithm (Press et al., 1992), and a weight  $w = 0.02$  is used in our implementation.

After the optimization for each key density  $g_k$ , a diffusion coefficient set and a modulation strength value set are obtained and listed in Table 1. Here,  $\hat{g}_k = g_k \cdot 255$  is the key density level and  $m(g)$  is the modulation strength value. The diffusion coefficients are defined by  $A_{100}$ ,  $A_{-110}$ ,  $A_{010}$ ,  $A_{0-11}$ ,  $A_{-101}$  and  $A_{001}$ :

$$\begin{aligned} d_{10}^{(x,y)} &= d_{10}^{(x,z)} = A_{100}(g)/M(g), & d_{-11}^{(x,y)} &= A_{-110}(g)/M(g), \\ d_{01}^{(x,y)} &= d_{10}^{(y,z)} = A_{010}(g)/M(g), & d_{-11}^{(y,z)} &= A_{0-11}(g)/M(g), \\ d_{01}^{(x,z)} &= d_{01}^{(y,z)} = A_{001}(g)/M(g), & d_{-11}^{(x,z)} &= A_{-101}(g)/M(g), \end{aligned}$$

where  $M(g) = A_{100} + A_{-110} + A_{010} + A_{0-11} + A_{-101} + A_{001}$ . It can be found that some values of modulation strength  $m(g)$  is slightly larger than 1.0. This is acceptable because it simply amplifies the energy of the added white noise. According to our experiments, that can help to achieve better symmetry of the Fourier power spectrum, and is not harmful to the obtained sampling result (Knox and Eschbach, 1993; Zhou and Fang, 2003).

For other density levels, the optimal parameters can be quickly calculated by a linear interpolation between their two adjacent key density levels.

Table 2: The average sampling efficiency of our method and 3D Poisson disk sampling methods (The volume data size in our method is  $128^3$ ).

Method	Number of samples per second (3D)
(Gamito and Maddock, 2009)	$10^3 \sim 10^4$
(Ebeida et al., 2012)	$7.5 \times 10^4$
Our method	$10^6 \sim 10^7$

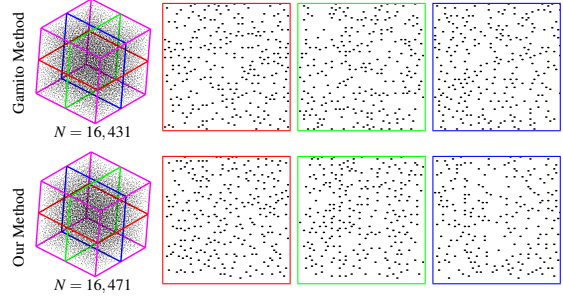
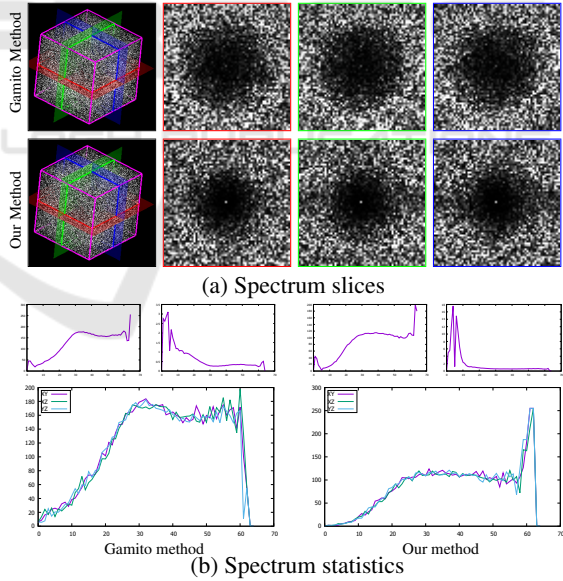

Figure 6: The sampling results using our method and 3D Poisson disk sampling method (Gamito and Maddock, 2009). The volume data is a  $64^3$  cube with a fixed sampling density of  $g = \frac{16}{255}$  in our method.  $N$  is the number of sampling results. Locations of the 2D slices are indicated by colors.


Figure 7: Comparison of our method with 3D Poisson disk sampling method (Gamito and Maddock, 2009) in terms of Fourier power spectrum slices and statistics. (a) 3D Fourier power spectrum slices of the sampling results (Fig.6). (b) Top: radially averaged power spectrum and anisotropy. Bottom: SRAPSs. The location of the 2D slices is indicated by colors.

## 5 EXPERIMENTAL RESULTS

With the optimized parameters, our 3D error-diffusion algorithm is able to generate sampling points with blue-noise distribution. We implement our sampling algorithm on a common PC with an Intel i7 3.4GHz CPU. In this section, experimental results of our algorithm are shown and analyzed.

### 5.1 Comparison with Poisson Disk Sampling

We compare our 3D error-diffusion sampling method with the Poisson disk sampling methods (Gamito and Maddock, 2009; Ebeida et al., 2012). In Table 2, we show the sampling efficiency of the two kind of methods.

In fact, the time complexity of our method is linear in the size of the input volume data, which is independent of the input data set. Therefore, the time complexity of our method is  $O(N')$ , where  $N' = L^3$  is the size of the volume data. However, the time complexity of the Poisson disk sampling method is correlated positively with the number of sampling points, and inversely with the disk radius. The time complexity of Poisson disk sampling is  $O(N \log N)$  in spatial subdivision (Gamito and Maddock, 2009) and empirical  $\Theta(N)$  in the flat quadtree method (Ebeida et al., 2012). Therefore, when the number of sampling points grows, the time cost of our method remains constant, while that of 3D Poisson disk sampling increases significantly.

The number of sampling points obtained by 3D error-diffusion is determined by the average density. For a volume data with fixed density level  $g$  and size of  $L^3$ , the expected number of sampling points  $N$  satisfies

$$N = g \cdot L^3. \quad (12)$$

Given the same number of sampling points, both kind of methods produce comparable sampling results (Fig.6). The Fourier power spectrums and their 2D slices demonstrate that the sampling points generated by both methods are uniformly and randomly distributed (Fig.7(b)), and their frequency spectrums are symmetrical and lack of low frequency component (Fig.7(a)). However, when inspecting the spectrums with the metrics defined in Section 4, we can find that the sampling results by our method achieve better blue-noise property. The SRAPS curves given in Fig.7(b) indicate that our results have better symmetries than the 3D Poisson disk sampling method.

### 5.2 Volume Data with Fixed Sampling Density

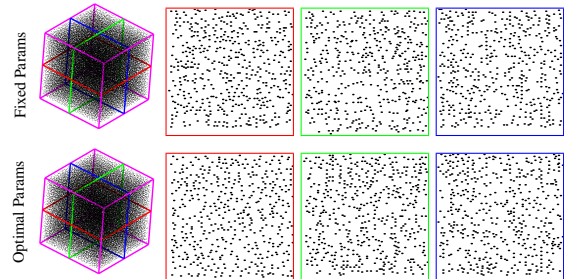


Figure 8: The sampling results using optimal parameters and fixed parameters. The input volume data has a fixed density  $g = \frac{8}{255}$  and the size of  $128^3$ . Locations of the 2D slices are indicated by colors.

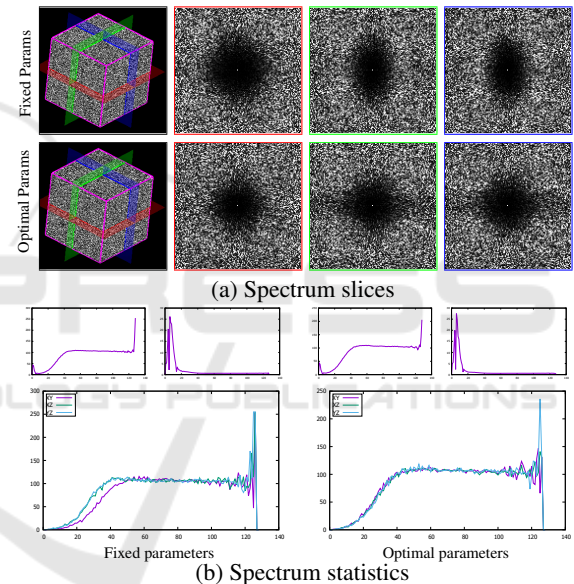


Figure 9: Comparison of optimal parameters with fixed parameters in terms of Fourier power spectrum slices and statistics. (a) 3D Fourier power spectrum slices of the sampling results (Fig.8). (b) Top: radially averaged power spectrum and anisotropy. Bottom: SRAPSs. The location of the 2D slices is indicated by colors.

To validate the effectiveness of our algorithm, we compare the 3D sampling results using the optimal variable parameters with that using the un-optimized fixed parameters. In Fig.8 (top), fixed parameters  $A_{100} = 4$ ,  $A_{.110} = 2$ ,  $A_{010} = 4$ ,  $A_{0.11} = 2$ ,  $A_{.101} = 2$ ,  $A_{001} = 2$ , and  $m(g) = 1.00$  is used for sampling. In this configuration, larger coefficients are given to the closer diffusion positions to the voxel being processed. In contrast, optimal parameters from Table 1 are used in Fig.8 (bottom). The spectrum statistical curves show that the optimal parameters play an important role in improving the symmetry of



Figure 10: Slices of 3D error-diffusion sampling to a  $64 \times 64 \times 256$  variable-density volume data. The density changes from 1 to 0 along the z axis. (a) XZ-Slice. (b) YZ-Slice.

the Fourier power spectrum. When considering the correlation of the SRAPSs (Fig.9 (b)), we can see that the optimal parameters lead to larger correlation value than the fixed parameters. Consequently, the spectrum using optimal parameters is more symmetric (Fig.9 (a)), and thus has better 3D blue-noise properties.

From the sampling point distribution shown in Fig.8, it can be found that there are less granular points clustering in the results using the optimal parameters than using the un-optimized ones. That is also a result of our optimization process which reduces the lower frequency component in Fourier power spectrums.

### 5.3 Volume Data with Variable Sampling Density

As illustrated in Fig.10, we apply 3D error-diffusion sampling to a set of volume data whose density gradually changes along one of the coordinate axes. From the 2D slices of the sampling result, we can see that the sampling points have uniform and random distribution.

Using 3D error-diffusion algorithm, we also perform importance sampling to several sets of complex 3D volume data according to their local features. First, the attribute information of each voxel in the volume data is converted into normalized sampling density level. The resulting sampling density function in the 3D volume space is taken as the input of our algorithm. Then, each voxel in the volume data uses different optimal parameters for quantization and error-diffusion, according to its corresponding sampling density. By this way, an importance sampling result, controlled by the sampling density function, can be obtained.

As shown in the experimental results in Fig.11, the sampling points are distributed uniformly in the 3D volume and maintain the structure features of the volume data. It can be seen that, the regions with salient features contain more sampling points and the smooth regions with less features have less sampling. With this effect, our method is able to reduce the number of voxels in the volume data while

maintaining the key features.

From the experimental results, a sampling point distribution satisfying 3D blue-noise property can be obtained. In low frequency region of the Fourier power spectrum, our method achieves better blue-noise property than 3D Poisson disk sampling method (Gamito and Maddock, 2009). In the high frequency region, our method can also guarantee the isotropic characteristics. Furthermore, the time cost of this sampling method is reduced compared with 3D Poisson disk sampling methods.

## 6 APPLICATIONS

The proposed 3D error-diffusion sampling method can be used for importance sampling, under the control of a sampling density function. Because of its high quality and high efficiency, this method may have many potential applications, such as volume rendering and tetrahedral meshing. In this section, we demonstrate the implementations and experimental results of our method in these application areas.

### 6.1 Volume Rendering

Since our 3D error-diffusion sampling method is able to produce blue-noise sampling point distribution, it can be used to improve the rendering quality for many volume rendering methods, e.g., the particle-based volume rendering (PBVR) method (Sakamoto et al., 2007). PBVR takes tiny particles as render primitives. The particles are generated from a given 3D scalar field based on a user-specified transfer function. Then, the final rendering results is calculated by projecting these particles onto the image plane.

In fact, the particles are essentially a group of random sampling points on 3D space according to the scalar field. In the original work of PBVR, they are generated in two ways: the hit-and-miss method (Sakamoto et al., 2007) or the Metropolis method (Metropolis et al., 1953). The former method performs sampling to discrete volume data. However, it can only produce white-noise sampling results, which do not possess the good properties of blue-noise distribution. Comparing with this method, using our 3D error-diffusion sampling may significantly improve the distribution of the particles, and hence better rendering results can be obtained as shown in Fig.12(b). The second method, i.e., the Metropolis method works in continuous domain and can produce particles with better distribution. But similar to the Poisson Disk sampling method, its computational cost is relatively high. In contrast, our sampling

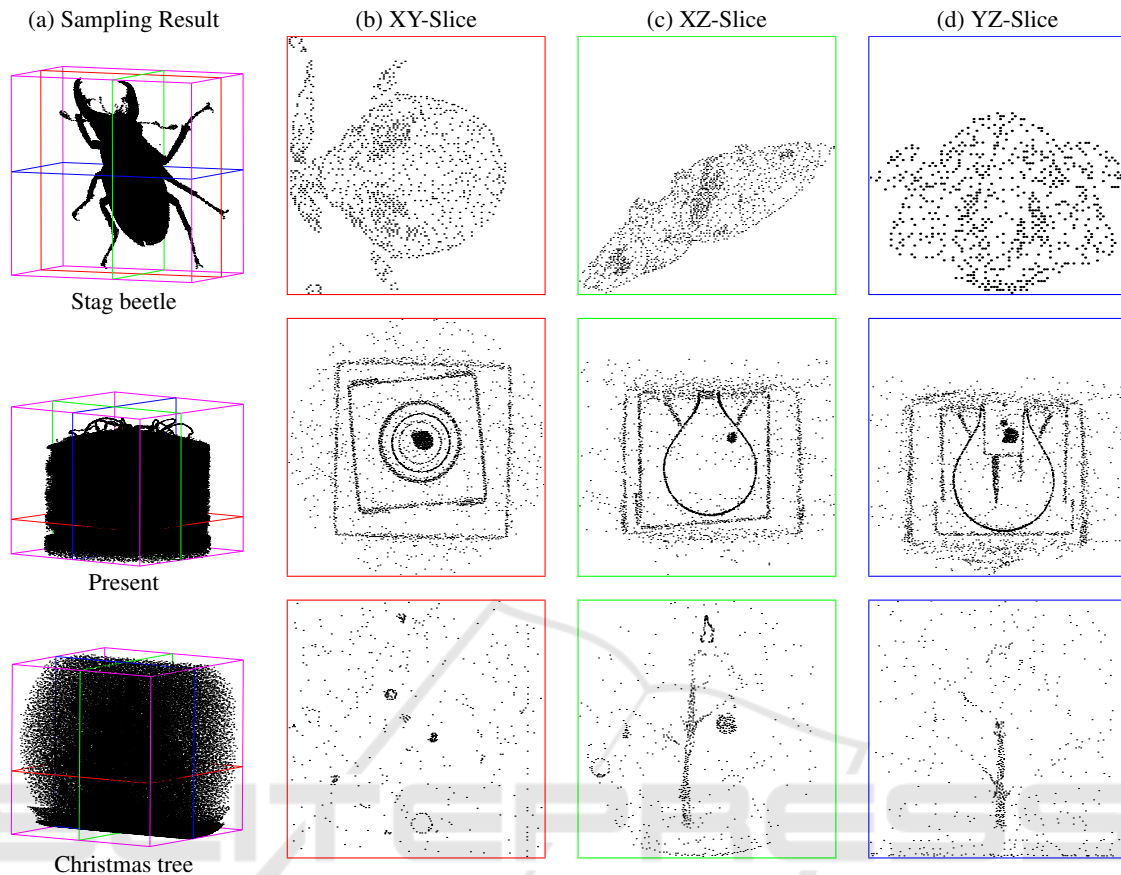


Figure 11: The 3D error-diffusion importance sampling results of variable-density volume data. The first column demonstrates the sampling points from three different volume datasets, and the corresponding volume slices are shown in the right columns. The volume datasets, Christmas Present (Heinzl, 2006), Stag Beetle (Gröller et al., 2005) and Christmas Tree (Kanitsar, 2002), courtesy of the Institut für computergraphik und Algorithmen, Technische Universität Wien.

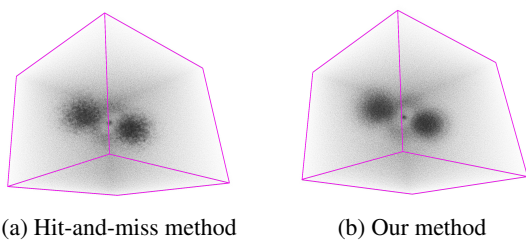


Figure 12: Particle-based volume rendering results, with particles generated by (a) Hit-and-miss method (Sakamoto et al., 2007) and (b) our 3D error-diffusion sampling method.

algorithm can guarantee the blue-noise property of the particle distribution while the computing efficiency is much higher.

In this way, our method can be applied to the areas of volume rendering, in which a random sampling point set on the volume with good distribution properties are necessary. Since our algorithm can effectively maintain the blue-noise property, the volume render-

ing methods utilizing our method can achieve better rendering results.

## 6.2 Volume Tetrahedral Meshing

In 2D image processing, vectorized image is a kind of compact representation, and becomes an effective alternative for traditional raster image. 2D image vectorization method generates triangular meshes on the image plane, based on a set of sampling points. Similarly, vectorized representation for volume data is also useful in many areas (Guo et al., 2016), and tetrahedral meshing is a widely used 3D vectorization method. First, a set of sampling points is generated by sampling to the volume data. Then, tetrahedral meshes are built from the sampling points. Obviously, the distribution property of the sampling points directly affects the quality of the meshes.

Therefore, we also implement a volume tetrahedral meshing method on the basis of our 3D error-

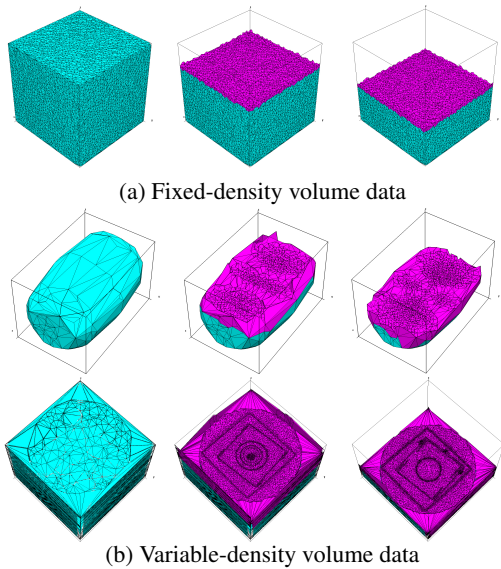


Figure 13: Volume tetrahedral meshing based on our 3D error-diffusion sampling points.

diffusion sampling method. The tetrahedral meshing is performed based on the sampling points generated by our method, and completed using the tools of TetGen (Si, 2015). Fig.13 shows the experimental results. First, a uniform tetrahedral mesh is built on the sampling result of a fixed-density volume data (Fig.13(a)). Then, two more complex tetrahedral meshes are constructed based on the importance sampling to the variable-density volume data (Fig.13(b)). From the sliced views of the tetrahedral meshes, we can see that the internal sampling points of the volume data are evenly distributed, hence the resulting meshes have a regular tetrahedral structure.

On the vertices of each tetrahedron, the attribute information of their corresponding original voxel, such as color or density, can be directly stored. In the internal of the tetrahedron, the attribute information of each voxel can be calculated by a fast interpolation according to the information stored on the four vertices of the tetrahedron. This therefore forms a vector expression of the original volume data. It can greatly reduce the storage of volume data, and hence improve the speed of volume transmission and rendering.

## 7 CONCLUSION

In this paper, a three-dimensional error-diffusion algorithm is described, which is an extension of the standard 2D error-diffusion. This algorithm can be used for sampling over volume data where a 3D discrete density function is defined at the voxels.

Similar with the tone-dependent 2D error-diffusion, our algorithm is density-dependent, i.e., the diffusion parameters are decided according to the density level of the voxel being processed. By defining the metric of 3D blue-noise property of sampling point distributions, a set of optimal parameters for 3D error-diffusion is obtained through an optimization process. The parameter set includes diffusion coefficients and threshold modulation strength values. Using the optimized parameters, our 3D error-diffusion can generate sampling points whose distribution possess blue-noise property. The generated sampling points shown in the bottom of Fig.8 possess a stochastic, evenness and isotropic distribution, which can be verified by Fig.9 (b). In this figure, the evenness and low level of radial anisotropy means there is no outlied higher spectrum in frequency domain, which is an indication of the property. The high correlation and lack of low frequency within SRAPSs is also an important indication of blue-noise property of the point distribution.

To explore the applications of our algorithm, experiments are also performed in the area of discrete volume data processing, including volume rendering, volume tetrahedral meshing. The results demonstrate that our algorithm can generate high quality sampling points with higher efficiency, and that can result in better rendering and tetrahedral meshing for volume data.

**Limitation and Future Work.** In our method, aliasing may occur at the beginning of the scanning of our algorithm. That is because the cumulative quantization error of the voxels is less than the diffusion threshold at the beginning of sampling. This transition effect should be further reduced in the future work.

Exploring volume rendering based on the sampling points will be another interesting future work. Sampling points with 3D blue-noise distribution, as well as corresponding tetrahedral meshes, can be easily obtained by our method. The attributes of the voxels inside a tetrahedron can be rapidly reconstructed by interpolation method, such as mean value coordinates (Ju et al., 2005). We will explore a fast volume rendering method based on such tetrahedral meshes, using new transfer functions, ray casting integral methods, and hardware acceleration. Furthermore, the tetrahedral meshes can be used to store and reconstruct the original volume data, and is useful in volume data compression.

## REFERENCES

- Alliez, P., Meyer, M., and Desbrun, M. (2002). Interactive geometry remeshing. *ACM Transactions on Graphics*, 21(3):347–354.
- Bourguignon, D., Chaine, R., Cani, M.-P., and Drettakis, G. (2004). Relief: A modeling by drawing tool. In *Proceedings of the First Eurographics Conference on Sketch-Based Interfaces and Modeling*, SBM'04, pages 151–160, Aire-la-Ville, Switzerland, Switzerland. Eurographics Association.
- Cohen, M. F., Shade, J., Hiller, S., and Deussen, O. (2003). Wang tiles for image and texture generation. *Acm Transactions on Graphics*, 22(3):287–294.
- Cook, R. L. (1986). Stochastic sampling in computer graphics. *Acm Transactions on Graphics*, 5(1):51–72.
- Csebfalvi, B. and Szirmay-Kalos, L. (2003). Monte carlo volume rendering. In *Proc. IEEE Visualization 2003*, pages 449–456.
- Dippé, M. A. Z. and Wold, E. H. (1985). Antialiasing through stochastic sampling. *SIGGRAPH Computer Graphics*, 19(3):69–78.
- Du, Q., Faber, V., and Gunzburger, M. (1999). Centroidal voronoi tessellations: Applications and algorithms. *SIAM Review*, 41:637–676.
- Ebeida, M. S., Davidson, A. A., Patney, A., Knupp, P. M., Mitchell, S. A., and Owens, J. D. (2011). Efficient maximal poisson-disk sampling. *Acm Transactions on Graphics*, 30(4):76–79.
- Ebeida, M. S., Mitchell, S. A., Patney, A., Davidson, A. A., and Owens, J. D. (2012). A simple algorithm for maximal poisson-disk sampling in high dimensions. *Computer Graphics Forum*, 31(2):785–794.
- Floyd, R. W. and Steinberg, L. (1976). An Adaptive Algorithm for Spatial Greyscale. *Proceedings of the Society for Information Display*, 17(2):75–77.
- Gamito, M. N. and Maddock, S. C. (2009). Accurate multidimensional poisson-disk sampling. *ACM Transactions on Graphics*, 29(1):8:1–8:19.
- Gonzalez, R. C., Woods, R. E., and Eddins, S. L. (2004). Digital image processing using matlab. *Ann.rev.fluid Mech*, 21(84):197–199.
- Gröller, M. E., Glaeser, G., and Kastner, J. (2005). Stag beetle dataset. <https://www.cg.tuwien.ac.at/research/publications/2005/dataset-stagbeetle/>.
- Guo, J., Yan, D. M., Chen, L., Zhang, X., Deussen, O., and Wonka, P. (2016). Tetrahedral meshing via maximal poisson-disk sampling. *Computer Aided Geometric Design*, 43:186–199.
- Heinzl, C. (2006). Christmas present dataset. <https://www.cg.tuwien.ac.at/research/publications/2006/dataset-present/>.
- Jiang, M., Zhou, Y., Wang, R., Southern, R., and Zhang, J. J. (2015). Blue noise sampling using an sph-based method. *ACM Transactions on Graphics (TOG)*, 34(6):211.
- Ju, T., Schaefer, S., and Warren, J. (2005). Mean value coordinates for closed triangular meshes. *ACM Transactions on Graphics*, 24(3):561–566.
- Kanitsar, A. (2002). Christmas tree dataset. <https://www.cg.tuwien.ac.at/research/publications/2002/dataset-christmastree/>.
- Kim, S. Y., Maciejewski, R., Isenberg, T., Andrews, W. M., Chen, W., Sousa, M. C., and Ebert, D. S. (2009). Stippling by example. In *Proc. the 7th International Symposium on Non-Photorealistic Animation and Rendering*, NPAR '09, pages 41–50.
- Knox, K. T. and Eschbach, R. (1993). Threshold modulation in error diffusion. *Journal of Electronic Imaging*, 2(3):185–192.
- Metropolis, N., Rosenbluth, A. W., Rosenbluth, M. N., Teller, A. H., and Teller, E. (1953). Equation of state calculations by fast computing machines. *Journal of Chemical Physics*, 21(6):1087–1092.
- Novelline and Fisher, M. (2004). Squire's fundamentals of radiology, 6th ed.
- Ostromoukhov, V. (2001). A simple and efficient error-diffusion algorithm. In *Proc. the 28th Annual Conference on Computer Graphics and Interactive Techniques*, SIGGRAPH '01, pages 567–572, New York, NY, USA. ACM.
- Ostromoukhov, V., Donohue, C., and Jodoin, P.-M. (2004). Fast hierarchical importance sampling with blue noise properties. *ACM Transactions on Graphics*, 23(3):488–495.
- Press, W. H., Teukolsky, S. A., Vetterling, W. T., and Flannery, B. P. (1992). *Numerical Recipes in C (2nd Ed.): The Art of Scientific Computing*. Cambridge University Press, New York, NY, USA.
- Sakamoto, N., Nonaka, J., Koyamada, K., and Tanaka, S. (2007). Particle-based volume rendering. In *Proc. Int'l Asia-Pacific Symposium on Visualization 2007*, APVIS '07, pages 129–132.
- Si, H. (2015). Tetgen, a delaunay-based quality tetrahedral mesh generator. *ACM Trans. Math. Softw.*, 41(2):11:1–11:36.
- Ulichney, R. (1987). *Digital Halftoning*. MIT Press, Cambridge, MA.
- Wei, L.-Y. (2008). Parallel poisson disk sampling. *ACM Transactions on Graphics*, 27(3):20:1–20:9.
- White, K. B., Cline, D., and Egbert, P. K. (2007). Poisson disk point sets by hierarchical dart throwing. In *Proc. IEEE Symposium on Interactive Ray Tracing*, pages 129–132.
- Yan, D.-M., Guo, J.-W., Wang, B., Zhang, X.-P., and Wonka, P. (2015). A survey of blue-noise sampling and its applications. *Journal of Computer Science and Technology*, 30(3):439–452.
- Zhong, Z. and Hua, J. (2016). Kernel-based adaptive sampling for image reconstruction and meshing. *Computer Aided Geometric Design*, 43:68–81.
- Zhou, B. and Fang, X. (2003). Improving mid-tone quality of variable-coefficient error diffusion using threshold modulation. *ACM Transactions on Graphics*, 22(3):437–444.

## APPENDIX

### Derivation of the Principal Frequency

When density  $g$  of input volume data satisfies  $0 \leq g \leq 0.5$ , average distance between sampling points is called the principal wavelength (Ulichney, 1987). If the principal wavelength is  $\lambda_g$ , average volume occupied by each sampling point is  $\lambda_g^3$ . Therefore, the number  $N$  of sampling points can be expressed by following Eq.13:

$$N = \frac{L^3}{\lambda_g^3} \quad (13)$$

where  $L$  is the size of the volume data. The number  $N$  of sampling points can be obtained by Eq.12. Therefore, the principal wavelength is derived as following by equal of Eq.12 and Eq.13:

$$\lambda_g = \frac{1}{\sqrt[3]{g}} \quad (14)$$

where the density  $g$  satisfies  $0 \leq g \leq 0.5$ . Because the principal frequency is the reciprocal of the principal wavelength (Ulichney, 1987), the principal frequency  $f_g$  is described as follow:

$$f_g = \sqrt[3]{g}. \quad (15)$$

Also, principal frequency  $f_g$  can be obtained easily when density  $g \in [0.5, 1]$ . Therefore, the principal frequency  $f_g$  is described as Eq.6.